SAND2014-20043C

Object Composition Identification via Mediated-Reality Supplemented Radiographs

Edward S. Jimenez, *Member, IEEE,* Laurel J. Orr, *Member, IEEE,* Kyle R. Thompson, *Member, IEEE*

***Abstract*—This exploratory work investigates the feasibility of extracting linear attenuation functions with respect to energy from a multi-channel radiograph of an object of interest composed of a homogeneous material by simulating the entire imaging system combined with a digital phantom of the object of interest and leveraging this information along with the acquired multi-channel image. This synergistic combination of information allows for improved estimates on not only the attenuation for an effective energy, but for the entire spectrum of energy that is coincident with the detector elements. Material composition identification from radiographs would have wide applications in both medicine and industry. This work will focus on industrial radiography applications and will analyse a range of materials that vary in attenuative properties. This work shows that using iterative solvers holds encouraging potential to fully solve for the linear attenuation profile for the object and material of interest when the imaging system is characterized with respect to initial source x-ray energy spectrum, scan geometry, and accurate digital phantom.**

I. Introduction

Full system characterization has been leveraged successfully for various estimation tasks in works [1], [2] related to SPECT imaging as well as for applications in optical testing [3]. Past work described a simplistic approach to estimate effective attenuation coefficients which reasonably estimated effective attenuation values for various low-attenuation but failed for higher-attenuation materials [4]. The main cause of the breakdown in this simplistic approach seemed to be mainly related to the lack of consideration to the non-linearities in the formation of the radiograph. Additionally, a more sophisticated approach to approximate attenuation information failed to consistently approximate materials due to the presence of null-spaces in the simulated imaging system [5].

II. Approach

We represent the discretized approximation to the initial energy profile of the source adjusted for attenuation through air as:

$$I_0(\epsilon)|_{\vec{\varepsilon}} \approx \vec{\rho} \in \mathbb{R}^m,\ \epsilon \in \mathbb{R}$$

E.S. Jimenez is at Sandia National Laboratories Software Systems R&D in Albuquerque NM 87185-0933 USA (telephone: 505-284-9690 email: esjimen@sandia.gov

L.J. Orr is at Sandia National Laboratories Software Systems R&D in Albuquerque NM 87185-0932 USA (email: ljorr@sandia.gov

K.R. Thompson is at Sandia National Laboratories Structural Dynamics & X-ray Non-Destructive Evaluation in Albuquerque NM 87185-0555 USA (email: krthomp@sandia.gov

where each component ρ_i is approximately equal to $I_0(\varepsilon_i)$ and ε_i is some sample point within the domain of ϵ and satisfies the following ordering:

$$\varepsilon_{i-1} < \varepsilon_i < \varepsilon_{i+1}.$$

Therefore, the j^{th} pixel of the radiograph may be approximated as:

$$\vec{\rho}_j^{\,t} \begin{bmatrix} e^{-\mu(\varepsilon_1)x_j} \\ e^{-\mu(\varepsilon_2)x_j} \\ \vdots \\ e^{-\mu(\varepsilon_N)x_j} \end{bmatrix} = \vec{\rho}_j^{\,t} \vec{e}_j = I_j,$$

where x_j is the length of the j^{th} ray path from source to the j^{th} pixel intersected with the digital phantom. Note that each $\vec{\rho_j}$ will vary slightly when accounting for attenuation through air as the path length to each pixel vary as well as variation due to path length though the object of interest. Thus, leveraging every pixel in image I, we have the following system of equations:

$$\begin{bmatrix} \vec{\rho}_1^{\,t} & \vec{0} & \dots & \dots & \vec{0} \\ \vec{0} & \vec{\rho}_2^{\,t} & \vec{0} & \dots & \vec{0} \\ \vdots & \vec{0} & \ddots & \ddots & \vdots \\ \vdots & \vdots & \ddots & \vec{\rho}_{N-1}^{\,t} & \vec{0} \\ \vec{0} & \dots & \dots & \vec{0} & \vec{\rho}_N^{\,t} \end{bmatrix} \begin{bmatrix} \vec{e}_1 \\ \vec{e}_2 \\ \vdots \\ \vec{e}_N \end{bmatrix} = \mathbf{P}\vec{e} = \vec{\mathbf{I}},$$

where $\vec{0}$ is a zero vector with the same dimensionality as vector $\vec{\rho}^{\,t}$ and $\mathbf{P} \in \mathbb{R}^{N \times Nm}$. Solving $\mathbf{P}\vec{e} = \mathbf{I}$ can be done in a least-squares sense using any linear solver if $\mathbf{P}$ is full-rank; if not, iterative approaches must be used.

This work extends the exploratory work in [5] where using a direct search method (DSM) as a robust and straightforward method to approximate the attenuation profile of the object of interest by leveraging a multi-channel imaging detector instead of a single-channel detector that was studied previously [4], [5]. The estimation method is then applied to each binned image independently.

The DSM leveraged is the Nelder-Mead DSM [6], a robust gradient-free algorithm. The search method will approximate the attenuation profile for each channel as the sum of the first five Legendre Polynomials:

$$\hat{\mu}(\varepsilon) = \sum_{i=0}^{4} c_i p_i(\varepsilon),$$

where c_i for $i \in [0, 1, 2, 3, 4]$ are the parameters to be optimized with respect to the objective function, $p_i(\varepsilon)$ is the i^{th} Legendre Polynomial where the domain for the given energy bin is scaled to the interval $[-1, 1]$ to preserve orthogonality and thus numerical stability.

III. Implementation

Even if $I_0(\epsilon)$ is unfiltered, the matrix $\mathbf{P}$ will almost certainly not be full-rank if one factors in attenuation due to air.

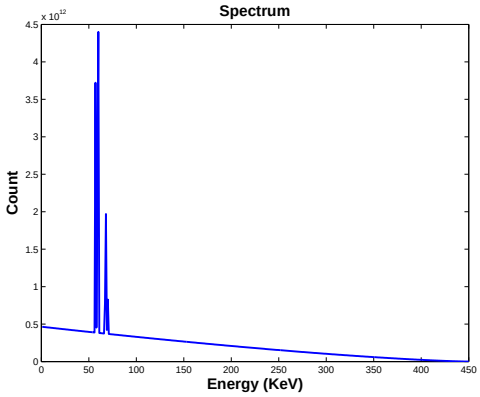

Figure 1. Simulated Spectrum

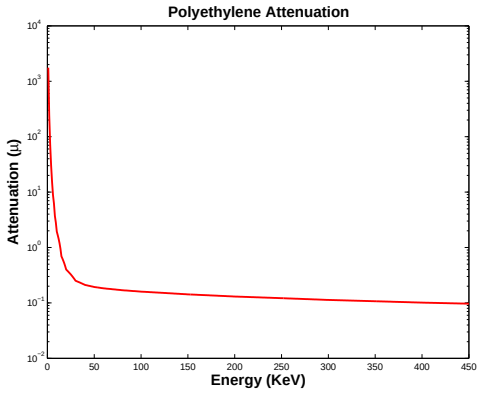

Figure 2. Simulated Attenuation

The example in this work is simulated in Matlab with attenuation data acquired from NIST [7]. An ideal detector is assumed as one could simply adjust the input spectrum to account for absorption in the scintillation material and any other related interactions. The example is assumed to be noise-free for this work with a Bremsstrahlung radiation source consisting of a Tungsten target with energies up to 450 KeV unfiltered. The object being imaged is an 11 sphere digital phantom all composed entirely of a single material with uniform

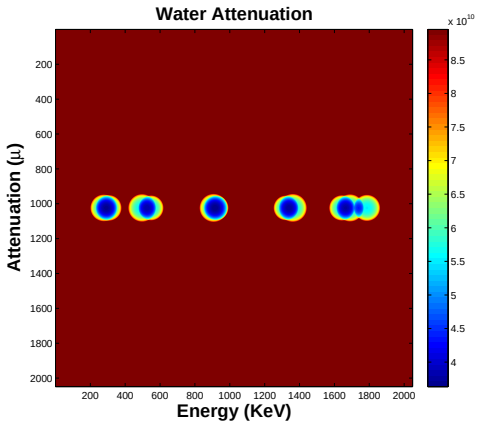

Figure 3. Simulated Radiograph

density and consistency with a spherical diameter of 2.5 cm arranged in a circular orientation. The radiograph is acquired using a source-to-detector distance of 225.66cm, an source-to-object distance of 188.3cm, a pixel pitch of 0.02cm and a 2048x2048 pixel detector.

This work will leverage the built-in Matlab Nelder-Mead DSM algorithm in the Matlab function *fminsearch* with generous maximum iterations of approximately 2.0×10^9 and maximum function evaluations of approximately 4.0×10^{11} to ensure that some local minima is reached; if either limitation is reached, a new initial guess will be given and the computation will be restarted.

IV. Evaluation

For this summary, this work attempts to solve for the attenuation profile for objects composted of:

- Copper
- Polyethylene
- Tin
- Water
- Lead

We will show three implementations of Nelder-Mead. The first is an unconstrained optimization. The second is an optimization method where only generally decreasing solutions are allowed. The last is constrained to be generally decreasing as well as strict boundary conditions in which the lower boundary must be the most attenuative value and the higher boundary corresponds to the lowest attenuation in the channel. Visual comparisons will be made for each estimated profile with its true solution. Lastly, convergence rates of the DSM will be presented.

V. Results

A. Unconstrained

Figures 4, 5, 6, 7, and 8 are the estimates for each material using an unconstrained Nelder-Mead DSM approach. The unconstrained approach yielded decent visual approximations thus potentially indicating that there may not exist many local minima that deviate significantly from the true solution. The computation

time for each estimate was approximately 90 minutes. It is clear that for higher attenuative materials (Pb, Sn, can Cu), there exist artifacts in the approximations that are not representative of real-world attenuation profiles. For all estimation methods, it seems that the low channels are at least partially occupying a null-space region of the imaging operator.

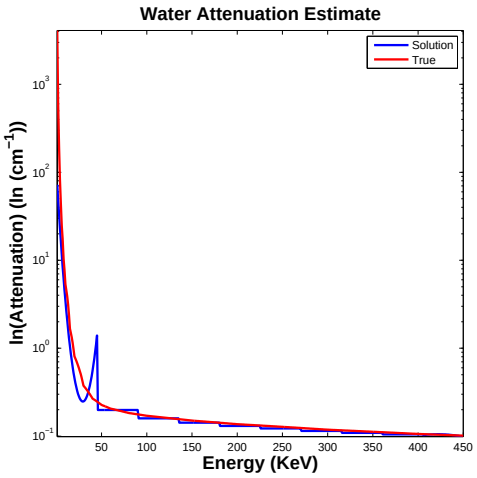

Figure 4. Unconstrained estimate for Water

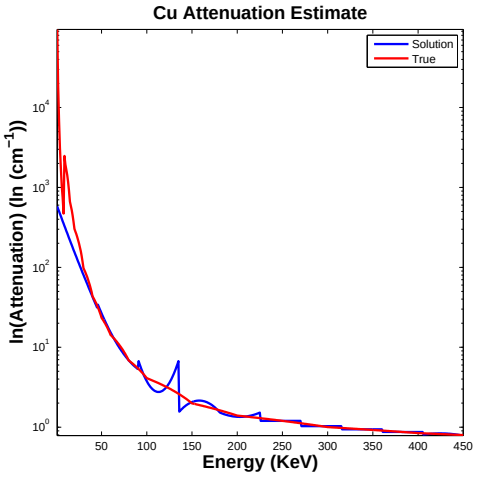

Figure 5. Unconstrained estimate for Copper

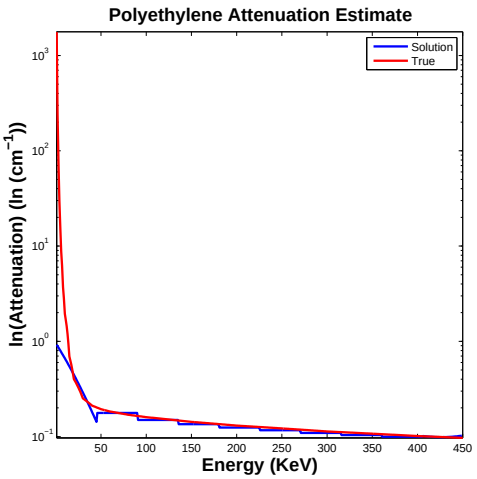

Figure 6. Unconstrained estimate for Polyethylene

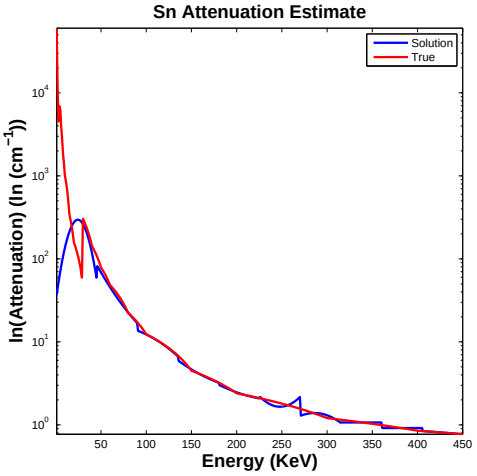

Figure 7. Unconstrained estimate for Tin

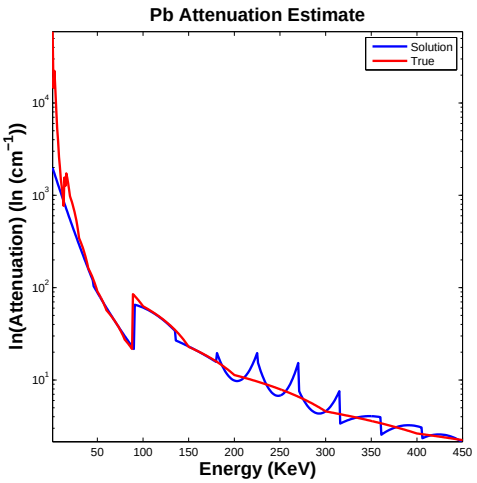

Figure 8. Unconstrained estimate for Lead

B. Generally Decreasing Constraint

Figures 9, 10, 11, 12, and 13 are the estimates for each material using the generally decreasing constraint. This constraint did not improve estimates by any appreciable amount, and in the case of Tin, the estimate was worse with respect to the presence of artifacts in the higher channels.

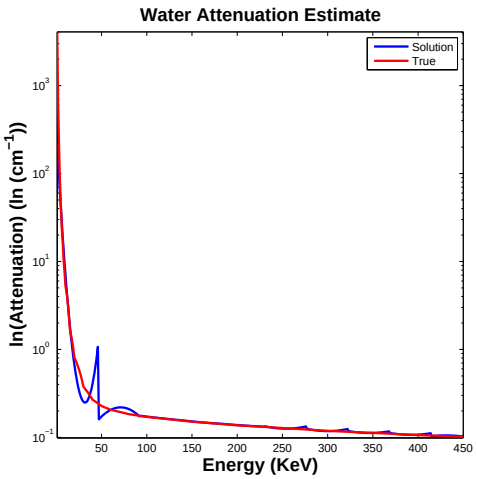

Figure 9. Decreasing constraint estimate for Water

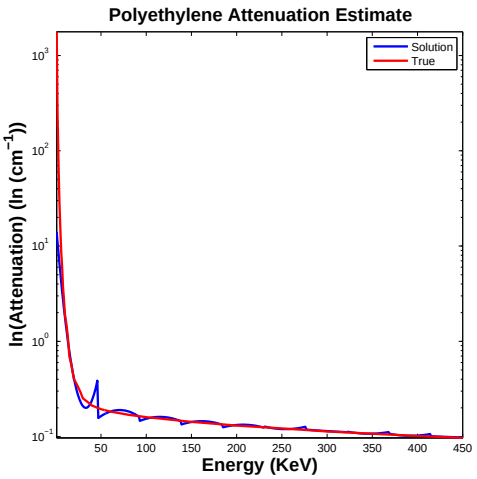

Figure 11. Decreasing constraint estimate for Polyethylene

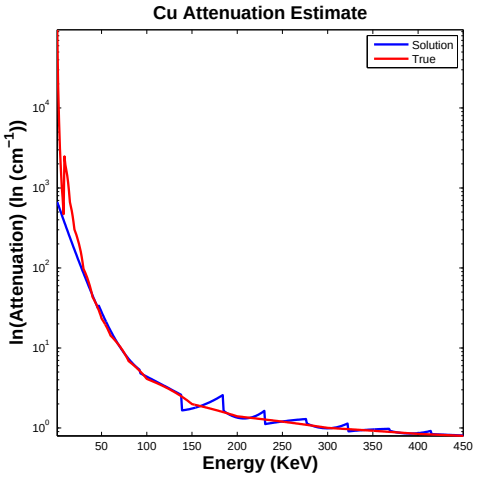

Figure 10. Decreasing constraint estimate for Copper

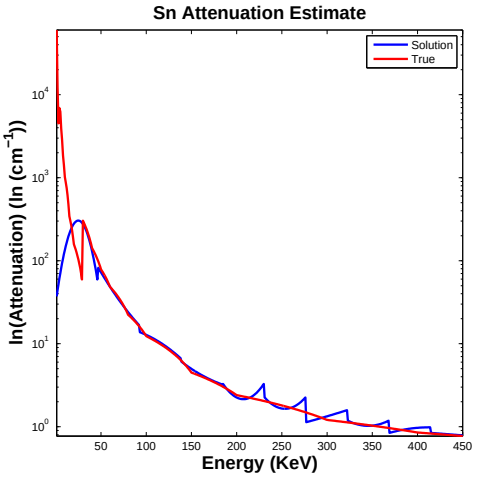

Figure 12. Decreasing constraint estimate for Tin

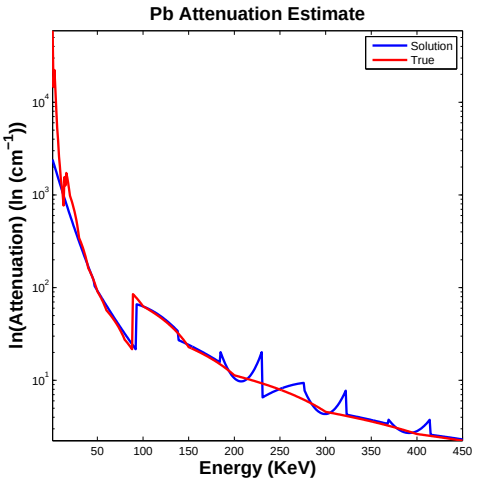

Figure 13. Decreasing constraint estimate for Lead

C. Boundary and Decreasing Constraints

Figures 14, 15, 16, 17, and 18 are the estimates for each material using the decreasing and boundary constraints. These estimates are the best fitting estimates visually. Although not completely eliminated, the artifacts are significantly suppressed. In the cases of the higher attenuative materials, the estimates are extremely close. In particular, the k-edge in Lead is fully resolved!. This requires additional investigation as it may just be a coincidence since the k-edge is near an interface point between energy channels for this example.

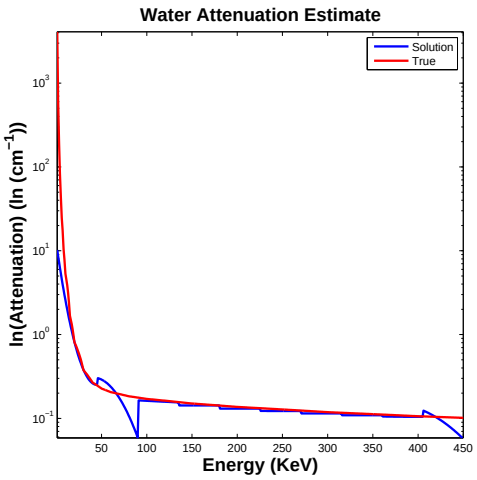

Figure 14. Decreasing and boundary constraint estimate for Water

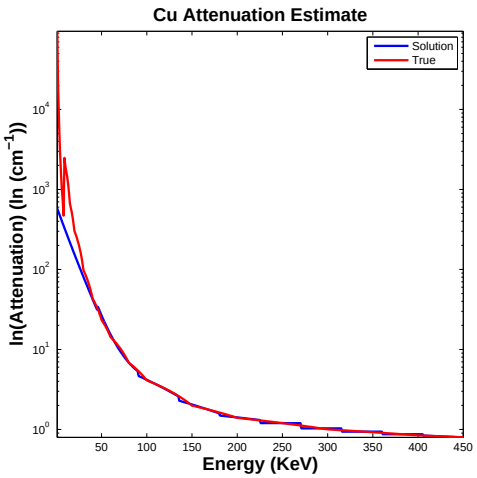

Figure 15. Decreasing and boundary constraint estimate for Copper

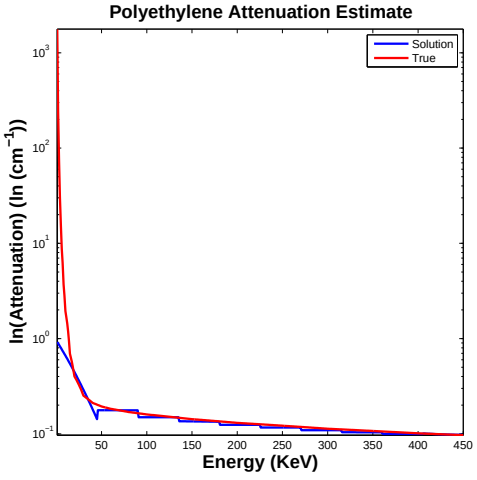

Figure 16. Decreasing and boundary constraint estimate for Polyethylene

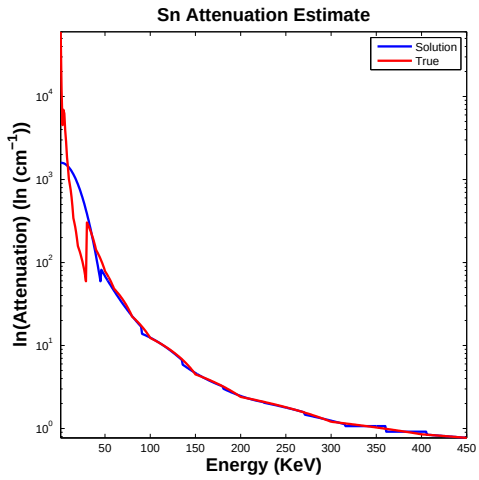

Figure 17. Decreasing and boundary constraint estimate for Tin

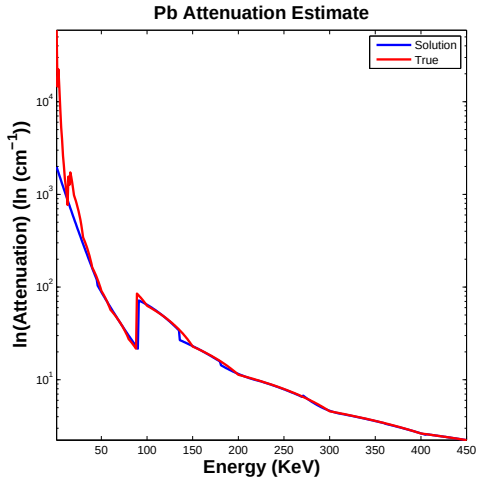

Figure 18. Decreasing and boundary constraint estimate for Lead

D. Rate-of-Convergence

Since the DSM algorithm is executed for each channel for each material, convergence rates for channels 1,5, and 10 for Pb estimation are presented as the performance was equivalent across all materials for each channel. Note that figures 19, 20, and 21 show convergence rates for channels 1, 5, and 10 respectively and none of these channels required more then 2500 iterations, well below the threshold set above; this was generally representative across all materials, none of which reached the iteration or function evaluation limits. Wall-time computational performance ranged from 5-15 minutes per channel across all materials.

VI. Conclusion

We have drastically improved attenuation profile estimation from radiographs compared to [5] and [4]

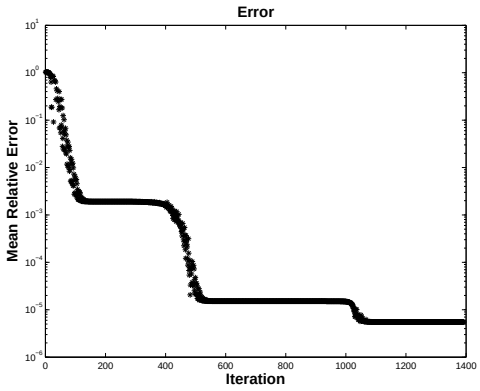

Figure 19. Relative error with respect to DSM iterations for thel 1^{st} profile estimation of Pb.

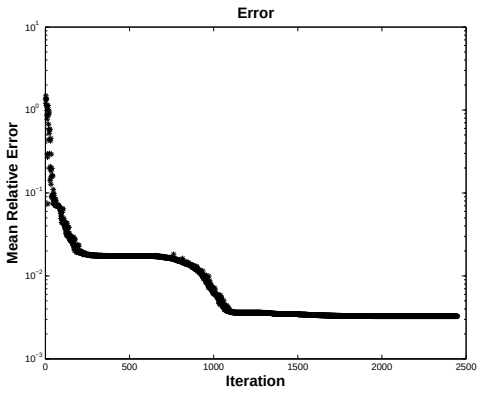

Figure 20. Relative error with respect to DSM iterations for the 5^{th} profile estimation of Pb.

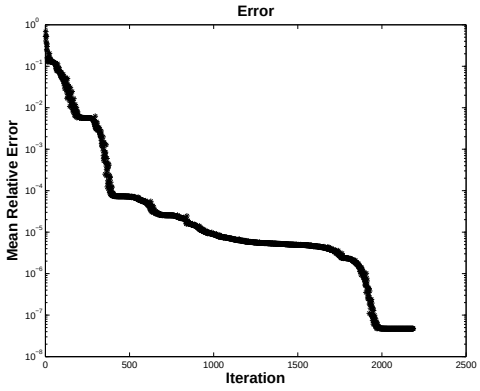

Figure 21. Relative error with respect to DSM iterations for the 10^{th} profile estimation of Pb.

by leveraging a multi-channel imaging detector. The estimation and identification of materials present in a radiograph or x-ray image has wide applications to non-destructive evaluation, medicine, quality assurance, and security. Our method leverages additional information including the pixel information and combines it to improve the performance of the estimation task. The performance is dependent on the quality of the characterization of the entire imaging system. If the imaging system is characterized accurately, it has been shown in previous work that the information could improve many estimation tasks [1]–[3]. Due to the exploratory nature of this work, the future work is extensive; this includes the addition of system and photon noise and fluorescence, object segmentation/support estimation, experimental evaluation and validation.

VII. Acknowledgements

Sandia National Laboratories is a multi-program laboratory managed and operated by Sandia Corporation, a wholly owned subsidiary of Lockheed Martin Corporation, for the U.S. Department of Energys National Nuclear Security Administration under contract DE-AC04-94AL85000.

References

[1] E. S. Jimenez, "Simulation and estimation of organ uptake in a digital mouse phantom," Ph.D. dissertation, The University of Arizona, 2010.

[2] Y. Chen, "System calibration and image reconstruction for a new small-animal spect system," Ph.D. dissertation, The University of Arizona, 2006.

[3] R. Park, "Novel applications using maximum-likelihood estimation in optical metrology and nuclear medical imaging: Point-diffraction interferometry and bazookapet," Ph.D. dissertation, The University of Arizona, 2014.

[4] E. S. Jimenez, K. R. Thompson, and L. J. Orr, "Utilization of virtualized environments for efficient x-ray attenuation approximation," in *ASNT Research Symposium*, Mar. 2014.

[5] M. L. M. Edward S. Jimenez, Laurel J. Orr and K. R. Thompson, "Exploring mediated reality to approximate x-ray attenuation coefficients from radiographs," in *Penetrating Radiation Systems and Applications XIV at SPIE Optics+Photonics 2014*, Aug. 2014.

[6] J. A. Nelder and R. Mead, "A simplex method for function minimization," *Computer journal*, vol. 7, no. 4, pp. 308–313, 1965.

[7] J. Hubbel and S. Seltzer. (2013, Jun.) Tables of x-ray mass attenuation coefficients and mass energy-absorption coefficients from 1 kev to 20 mev for elements z = 1 to 92 and 48 additional substances of dosimetric interest. [Online]. Available: http://www.nist.gov/pml/data/xraycoef/